A Bayesian shifting method for uncertainty in the open-hole gamma ray log around casing points

Rachel H. Oughton[1,2], David A. Wooff[2], and Stephen A. O'Connor[3]

[1]Department of Earth Sciences, Durham University, South Road, Durham DH1 3LE, UK.
[2]Department of Mathematical Sciences, Durham University, South Road, Durham DH1 3LE, UK.
[3]Ikon GeoPressure, Rivergreen Centre, Aykley Heads, Durham DH1 5TS, UK.

Acknowledgements

Abstract

The wireline gamma ray log is sensitive to open-hole conditions, and in particular the diameter. This means that the log can jump at casing points. Although environmental corrections exist, they can fail at these points. We present a Bayesian method for deriving a new quantity, the shifted gamma ray index, that takes these shifts into account by fitting a piecewise linear function to open-hole data in a depth window around the casing point. Because it is Bayesian, the method enables us to assess our uncertainty about its performance. This method requires very little knowledge of the borehole or drilling conditions, but relies on the assumption that the lithology is consistent. Investigating the other wireline logs enables us to assess whether this assumption is valid. We demonstrate our method using well data from offshore mid-Norway.

1 Introduction

In the petroleum industry, the gamma ray (GR) log is used routinely to estimate the shale volume, (V_{shale}), which is the percentage of total rock volume made up of shale. This quantity is particularly useful in a conventional pore-pressure prediction workflow, where a normal compaction trend will be defined using data from shales only, usually sonic transit time (DT), density (RHOB), resistivity (RES) or seismic interval velocity. For more detail on pore-pressure prediction methods, see for example Zhang (2011) or Mouchet and Mitchell (1989).

Although the GR log is usually calibrated to a standard such as API units, its value depends on the position of the sensor, the dimensions of the borehole and various other factors, and so it is not necessarily a precise expression of the level of GR activity of the formation. The behaviour of the whole log is therefore used, often by standardising the log to $[0,1]$, creating a quantity called the gamma ray index, I_{GR}.

To be able to use the GR log to estimate the lithology, we must account for the effects of these other factors. The effects can be especially significant at casing points. At these depths drilling is stopped and casing is run and cemented, hydraulically isolating the open formations from the previous casing point to the current depth. The lowermost casing section (the shoe) is set in non-reservoir rock, often a shale, prior to starting drilling again with a smaller bit size. Different logging equipment may be used from this point, and the type or properties of the drilling mud may also be changed. For these reasons, there is commonly a sharp change in the behaviour of the open-hole GR log at a casing point. We present a method for taking into account these larger-scale changes to create a new quantity, the shifted gamma ray index S_{GR}. Our approach is based on detecting a change in mean at a known casing point, guided by prior information as to the depth of the casing point and the surrounding lithology.

In Section 2 we discuss the GR log in more detail, and briefly mention some existing methods for dealing with its uncertain nature. Our S_{GR} method is introduced in Section 3. This method makes use of the Gibbs sampler (a Bayesian sampling method), introduced in Appendix A. Section 3.1 explains the probability model behind our method. In Section 4 we introduce some methods for validating the assumptions underlying the shifted GR index. In Section 5, we demonstrate the methodology using data from offshore mid-Norway.

Ideally wireline logs provided as digital data files will already have had environmental corrections made to them (Serra and Serra, 2004), and therefore re-applying environmental corrections would be inappropriate. Information about environmental corrections, especially regarding the GR, is often lacking in the log header and so the recipient must seek a data-driven method to correc for shifts across casing points. The shifted GR method we present uses the data themselves to create a consistent GR index, and is therefore of use in such situations. In the example in Section 5 we use wireline log data from digital LAS (log ASCII standard) files, not knowing whether the GR log has been corrected or not. Because the log continues through the casing changes with no break or duplication it is clear that some data processing has taken place.

2   The gamma ray log

The GR log records the natural gamma radiation from radioactive isotopes of uranium, thorium and potassium, and their daughter isotopes, present in the formation most frequently in clay minerals. This log is almost always run on all wireline and logging while drilling (LWD) tools for lithology interpretation and correlation between logging runs. This paper focusses on the wireline GR data in open-hole condi-

tions, as opposed to the behaviour of the GR log as it goes from open hole to cased hole. The spectral GR log gives a separate value for each decay series, but the total count GR log, which will be our focus, gives their combined radioactivity. This quantity has various uses in petroleum geology, for example in sedimentology and in correlations between wells, but our concern is its use in pore-pressure prediction. Different types of rock are radioactive to different degrees. Among sedimentary rocks, shales tend to have the highest levels of radioactivity, so the GR is often used to interpret shale from other lithology (Rider, 1990; Thibal et al., 1999; Serra and Serra, 2004).

The *gamma ray index*, defined as

$$I_{GR} = \frac{GR - \min{(GR)}}{\max{(GR)} - \min{(GR)}},$$

is suggested by Asquith and Krygowski (2004) as a primitive but simple value for the shale volume. This relies on the assumption that although the GR values vary for different shales, within any particular well one would expect the GR value of a pure shale to be constant (Rider, 1996). Setting $V_{shale} = I_{GR}$ also implies that the shale content is proportional to the GR emissions, which may not be the case. Some non-linear calibration curves defining V_{shale} as a convex function of I_{GR} have been developed for formations of different ages (Bhuyan and Passey, 1994; Rider, 1996), and other relations have also been proposed for V_{shale}.

In many standard pore-pressure prediction workflows, (e.g. Eaton, 1975), a normal compaction trend must be defined, showing the decrease in shale porosity with depth under normal compaction where the pore-pressure is hydrostatic. The porosity in the formation is then compared to this curve to estimate pore-pressure (Mouchet and Mitchell, 1989). Since the porosity of a shale cannot easily be measured directly, data such as compressional sonic transit time (DT), deep resistivity (RES) and formation density (RHOB), as well as seismic interval velocity, are used as proxies for porosity. Where, for instance, high sonic transit times are measured by a wireline tool relative to the compaction trend, anomalous pore pressure is inferred.

The normal compaction trend is based on the assumption that shale lithology is consistent to enable the selection of shale intervals from the wireline log data (Swarbrick, 2002). The shale volume is usually used to do this, and so estimating V_{shale} is a critical part of the shale pore-pressure prediction workflow. Thus we must understand the GR log, where this is used as the primary shale indicator.

The GR log is very sensitive to borehole conditions and tool configuration (Maučec et al., 2009; Mendoza et al., 2006), and most of all borehole diameter (Chen, 1998). This can create large jumps in the GR log, particularly at casing points where the borehole diameter changes suddenly, leading to a misrepresentation of shale in the rock column, and potential inaccuracy in the final pressure prediction model. If too much shale is inferred then data that represent sands, for instance, may be incorporated in defining the normal compaction trend. This would lead to over-estimation of the pore pressure as the normal compaction curve would plot at faster velocity. Conversely, if too little shale is modelled, then

some key shale intervals may be assigned as sand and not used, and so degrade the definition of the compaction model. The variation in the GR from changes in these conditions can be far greater than the variation owing to changes in lithology (Bristow and Williamson, 1998). Before the GR log can be used to interpret the lithology, therefore, this issue must be addressed.

We review existing methods for taking into account uncertainty in the GR log before introducing our own Bayesian method, the shifted GR index.

2.1 Existing methods for correcting the GR log

Methods exist for correcting the gamma ray log to account for specific conditions, but they are mostly empirically derived, and include variables which may not be known. Serra and Serra (2004) give correction formulae for different Schlumberger logging tools and different borehole conditions, which include parameters relating to the casing (if present), pore fluid, mud properties, tool position within the borehole and borehole diameter. These parameters are used to calculate a parameter, t, and the correction factor is read from a plot showing correction factor against t for different tools, positions within the borehole (centred and eccentred) and drilling mud types. Note that since the shifted GR method concerns only open-hole data, casing and cement effects are irrelevant.

Lehmann (2010) collects together GR correction formulae that are used in the uranium mining industry. Each of these equations calculates a scale factor Y which is then applied to the raw data, such that $GR_{cor} = Y \cdot GR_{raw}$, where GR_{cor} is the corrected GR value. Different formulae are presented for Y, depending on whether there is casing or not, whether the pore fluid is water or oil, whether the GR sensor is centred or eccentred. The equations for Y involve the borehole fluid density and the borehole diameter, and each contains several empirically derived constants. Stromswold and Wilson (1981) also present correction formulae for the GR log, taking into account the variation in borehole fluid and diameter and the presence of steel casing. Weatherford (2009) gives GR corrections as graphs.

Although philosophically it is appealing to derive equations using physical reasoning, the exact values of the borehole geometry, drilling conditions, tool position and fluid properties may not be known, and their effects will not necessarily be as simple as assumed in the derivation of such equations. Furthermore, the correction methods discussed aim to realign the GR log to calibrated data (Stromswold and Wilson, 1981; Lehmann, 2010). The method we present in the following section aims simply to realign the GR log so that it is self-consistent and suitable for identifying zones of similar shale content to create normal compaction curves.

Since we do not know the tool type, position or diameter for the data used in the example, or indeed whether the data supplied have already been environmentally corrected as expected, we are unable to use the methods mentioned above to form a comparison. Because steps in the GR log response across casing points remain, even if environmental corrections have been applied, some form of shift correction

is still necessary for consistency in zonal identification.

3   The shifted gamma ray index

We propose a method that requires very little knowledge of the borehole conditions, but instead relies on some assumptions. For the method to be useful, these assumptions need to be reasonable, and we will look into ways of verifying them using other wireline logs.

The aim of this method is to account for the effect on the GR log of changes in borehole diameter and possibly in drilling mud and logging tool calibration that take place at casing points. The main underlying assumption is that the casing is set in a massive shale. This seems reasonable since Leak-Off Tests, which can only be performed in rocks of low porosity and permeability, are often performed just below the casing shoe (Mouchet and Mitchell, 1989), and it is desirable to change casing in a competent shale (Devereux, 1998). In the well-planning stages casing point selection can be informed by seismic data (Littleton et al., 2002) or through data from offset wells (Clouzea et al., 1998).

However, the assumption of a homogeneous shale could be verified by checking the mudlog and using other wireline logs such as RHOB and neutron porosity (NPHI) that are sensitive to lithology but less affected by casing points. The RHOB log is sensitive to borehole rugosity but is always accompanied by a caliper log and a delta-RHOB, both of which are useful for assessing the quality of the measurement. If NPHI is available then NPHI and RHOB can be used to interpret lithology, either to confirm or to contradict the assumption of a homogeneous shale. We will demonstrate some approaches in Section 4.

At each casing point (at depth z_{cas}), we fit a piecewise linear function like that in Figure 1 to the gamma ray data.

This is a simple model we use to estimate the effect of the casing point on the GR log, and the form was decided after studying GR logs that showed clear signs of being affected by casing points. Such signs can be seen in real data in Figure 3, which shows shifts in the GR logs around casing points for three offshore mid-Norway wells. The important features of the fitted function are the values of the open-hole GR log before and after the casing point, and the transition-zone: the region between z_{dtop} and z_{dbot}, where the GR log is not at either stable level. The transition-zone was introduced rather than an abrupt jump from one level to the next because, in most cases, the data showed a gradual change over the casing point from one level to the other, although this zone may often be very narrow. This may be a shoulder effect, as described by Rider (1996), or the result of data processing such as splicing or depth-matching the different log runs. Generally, the casing shoe is set a few metres above current bottomhole depth, leaving a small section of openhole often called the 'rathole'. The next section of borehole is then drilled with a smaller bit size. The transition zone should therefore cover this small section, the 'rathole', and only settle at a constant rate once the borehole is at the smaller diameter.
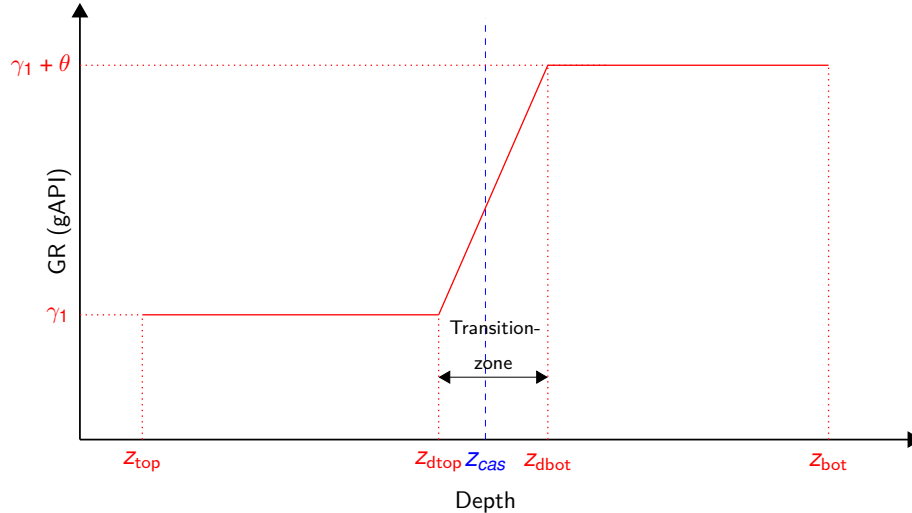
Figure 1: This shows the curve's parameters and the shape of the curve in relation to the casing point. The solid line is chosen to best fit the GR data around the casing point z_{cas}.

Theoretically one could rescale the data in the transition-zone using the fitted curve, however there are several problems with this. The transition zone part of the fitted curve has its own variance (τ_w^{-1} in what follows), which may be large if the data in the transition zone are highly variable or non-linear. This is a desirable property, allowing flexibility between the two constant portions of the curve whilst maintaining simplicity in the model. However, the poor fit of the curve would be likely to make it inadequate to transform the data. It is also common for there to be caving in the borehole immediately below the casing point, and this would cause the data to be of poor quality. One could investigate the caliper log to see whether this was the case. Instead we use the mean GR found by the model to connect the two constant portions.

The user is able to restrict the width of the transition-zone, and also to assess whether the model fit is appropriate. It should be emphasised that this method involves subjective choices to be made by the user. The nature of these choices is made clear in Section 3.1, and some examples of how the results depend on of the user's specifications are shown in Section 5.

The curve begins at $z = z_{\text{top}}$, and has a constant value γ_1 until $z = z_{\text{dtop}}$. From $z = z_{\text{dbot}}$ to $z = z_{\text{bot}}$ the curve has constant value $\gamma_1 + \theta$. For $z_{\text{dtop}} \leq z \leq z_{\text{dbot}}$, the function changes linearly from γ_1 to $\gamma_1 + \theta$. We refer to this region as the "transition-zone". Figure 2 shows an example using some real data.

In order to fit this curve to real data, we must estimate the parameters γ_1, θ, z_{dtop} and z_{dbot}. The depths z_{top} and z_{bot} will be fixed, but should not be outside the shale interval, and z_{cas} will be given. We use the depth of the casing shoe for z_{cas}, since this is the one most often given in well reports, although it is likely to be slightly shallower than the depth at which the borehole diameter changes. This is apparent in the examples, as z_{cas} is often very near the start of the transition-zone.
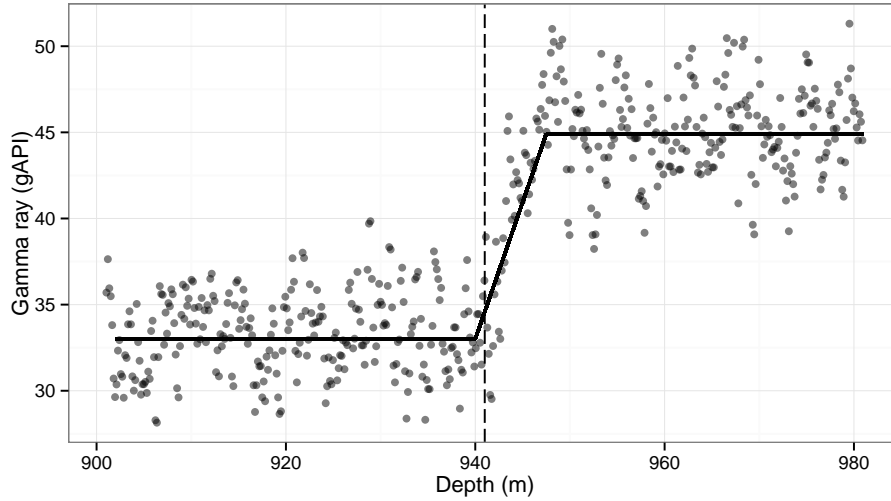
Figure 2: Piece-wise linear segments (solid line) as in Figure 1 are fitted to GR data from well 6305/8-1 around the casing point at 941m.

In allowing a transition-zone of uncertain width, this model extends from the problem of estimating the mean shift in a known-changepoint time series. Krishnaiah and Miao (1988) review least-squares regression, maximum-likelihood, and Bayesian approaches to that problem. For our extension we choose a Bayesian approach as it is straightforward to apply, appears to work well, and offers probabilistic updates of uncertainty for all parameters.

3.1 Fitting a piecewise linear function

The model described here is for the data around one casing point, at depth z_{cas}.

The algorithm requires some starting values:

d_{min} : the minimum length of the constant sections, that is of $z_{dtop} - z_{top}$ and $z_{bot} - z_{dbot}$,
 which restricts the width of the transition-zone;

d_{max} : the distance from z_{cas} to z_{top} and z_{bot} (assumed to be the same);

a, b, μ_p : hyperparameters for the prior distributions below.

The value of d_{max} should be chosen to cover an interval above and below the casing point in which the GR log appears to be approximately constant. In the examples that follow we used $d_{max} = 40m$ unless otherwise stated. The parameter dmin broadly controls how many observations are used to estimate the means for the constant segments preceding and succeeding the casing point. After some experimentation, we found that a value of $3m$ worked well for all our examples. A reasonable starting

7

choice for the parameter is the mean of the GR log between d_{min} and z_{cas}. In practice, the results we obtained were not sensitive to the value of when it was varied between 0 and 100. We used the values $a = 1$, $b = 1$ for all examples, to provide a non-informative prior distribution Carlin and Louis (2009).

We first establish a model for the likelihood:

$$GR_z \mid \gamma_1, \tau_v \sim N\left(\gamma_1,\ \tau_v^{-1}\right) \qquad\qquad \text{if } z_{top} < z < z_{dtop}$$

$$GR_z \mid \gamma_1, \theta, \tau_w \sim N\left(\gamma_1 + \theta\frac{z - z_{dtop}}{z_{dbot} - z_{dtop}},\ \tau_w^{-1}\right) \qquad\qquad \text{if } z_{dtop} < z < z_{dbot}$$

$$GR_z \mid \gamma_1, \theta, \tau_z \sim N\left(\gamma_1 + \theta,\ \tau_z^{-1}\right) \qquad\qquad \text{if } z_{dbot} < z < z_{bot}.$$

This stipulates that the GR data will be normally distributed about the curve we have described, and that the variances in the different sections (z_{top} to z_{dtop}, z_{dtop} to z_{dbot} and z_{dbot} to z_{bot}) may differ from one another. These variances are given by the precisions τ_v, τ_w, τ_z, and are considered unknown. Prior distributions must also be specified, and we use:

$$p\left(z_{dtop} = z\right) \propto \begin{cases} \frac{1}{k_1} & \text{if } (z_{top} + d_{min}) < z < z_{cas} \\ 0 & \text{otherwise} \end{cases}$$

$$p\left(z_{dbot} = z\right) \propto \begin{cases} \frac{1}{k_2} & \text{if } z_{cas} < z < (z_{bot} - d_{min}) \\ 0 & \text{otherwise} \end{cases}$$

$$\tau_v,\ \tau_w,\ \tau_z \sim \Gamma\left(a, b\right)$$

$$\gamma_1 \mid \tau_v \sim N\left(\mu_p, \tau_v^{-1}\right)$$

$$\theta \mid \tau_z \sim N\left(0, \tau_z^{-1}\right).$$

The top two distributions give equal probability to every permissible depth for z_{dtop} and z_{dbot}. The constants k_1 and k_2 are such that the probabilities sum to one. The precisions τ_v, τ_w and τ_z are forced to be positive by a Gamma distribution, which has density function

$$f\left(x\right) = \frac{1}{b^a \Gamma\left(a\right)} x^{a-1} e^{-x/b},$$

where the centre and spread are determined by the hyperparameters a and b. A prior mean must be given for γ_1, but a priori we expect $\theta = 0$. This would be simple to change.

Our aim is to combine data with this probability model to find the posterior probability distributions of the parameters, i.e. the distribution conditional on the data. Analytically this would be impossible, and so we use a Bayesian sampling tool, the Gibbs sampler, which we describe in Appendix A. The Gibbs sampler combines our prior model with the data (gamma ray data around a casing point) to produce samples from the posterior distributions of the model parameters γ_1, θ, z_{dtop}, z_{dbot}, τ_v, τ_w and τ_z.

At each casing point, the data in the transition-zone are removed, and the GR log below the transition-zone is shifted by the estimate of θ. Finally, as the absolute value of θ is arbitrary, we find S_{GR} by rescaling it to the interval $[0, 1]$, so that S_{GR} is analogous to I_{GR}.

Mathematically, this is no different from varying GR_{sand} and GR_{shale} above and below each casing point, which is common practice, but this method is not prone to arbitrary choices of the values and enables uncertainty analysis on the resulting log.

It may seem appealing to have a multiplicative element to the model. Indeed, many of the correction formulae given by Lehmann (2010), Weatherford (2009) and others are multiplicative. With this in mind, a multiplicative probability model was specified, where the constant part of the curve from z_{dbot} to z_{bot} was $\alpha\gamma_1 + \theta$. In this data-based approach, the only quantity with which we can estimate the scaling parameter α is the variance of the GR log. Therefore, rather than having three separate and independent variances, as in the probability model above, there was one variance, τ^{-1}, which was then scaled by α.

When this model was applied to real data it was clear that too much weight was being given to the variance, with previously significant features of the GR logs being lost. The additional parameter also made convergence of the Gibbs sampler much slower.

As stated in the introduction, the wireline logs in the digital data files should have already had environmental corrections made to them. In the case of the GR log, these would be likely to be multiplicative as we have seen.

4 Validating our assumptions

According to Rider (1996), RHOB, DT, NPHI and photo-electric effect (PEF) logs can all be used quantitatively (or semi-quantitatively) to interpret lithology. Therefore we will use these logs, where available, to validate (or expose as false) our assumption that the lithology around the casing point is homogeneous. The GR log is among the most available of the wireline logs, and is usually recorded over almost all of the well, along with the resistivity, sonic transit time and caliper logs. The caliper log in particular is useful for quality control, since if it shows rugosity in the borehole the other wireline logs are likely to be affected. Neutron porosity and density logs are typically run over shorter intervals around the reservoir. It may therefore be that over some casing points we have a limited selection of logs to study.

The first step will be to confirm that the casing point does not affect each log. We will do this by using the same function-fitting procedure as for the GR, except that now our concern is whether the posterior estimates for θ differ significantly from zero.

Secondly, assuming no casing point effect has been found, we must use the logs to interpret the lithology around the casing point. Hearst et al. (2000) suggested cross-plotting NPHI against RHOB. Where these logs are available we will do this, to check that all logged depth points around the casing shoe lie in the same lithological region of the NPHI-RHOB cross-plot. We will use some of these methods on real

data in Section 5.4.

5   Example: Offshore Mid-Norway

To demonstrate S_{GR} in practice, we will use some wells from offshore mid-Norway, whose GR data and casing points are shown in Figure 3. In Section 5.4 we will use the other logs, as described in Section 4, to back up our use of S_{GR}.


(a) Well 6406/1-1   **(b)** Well 6506/11-7   **(c)** Well 6406/2-7
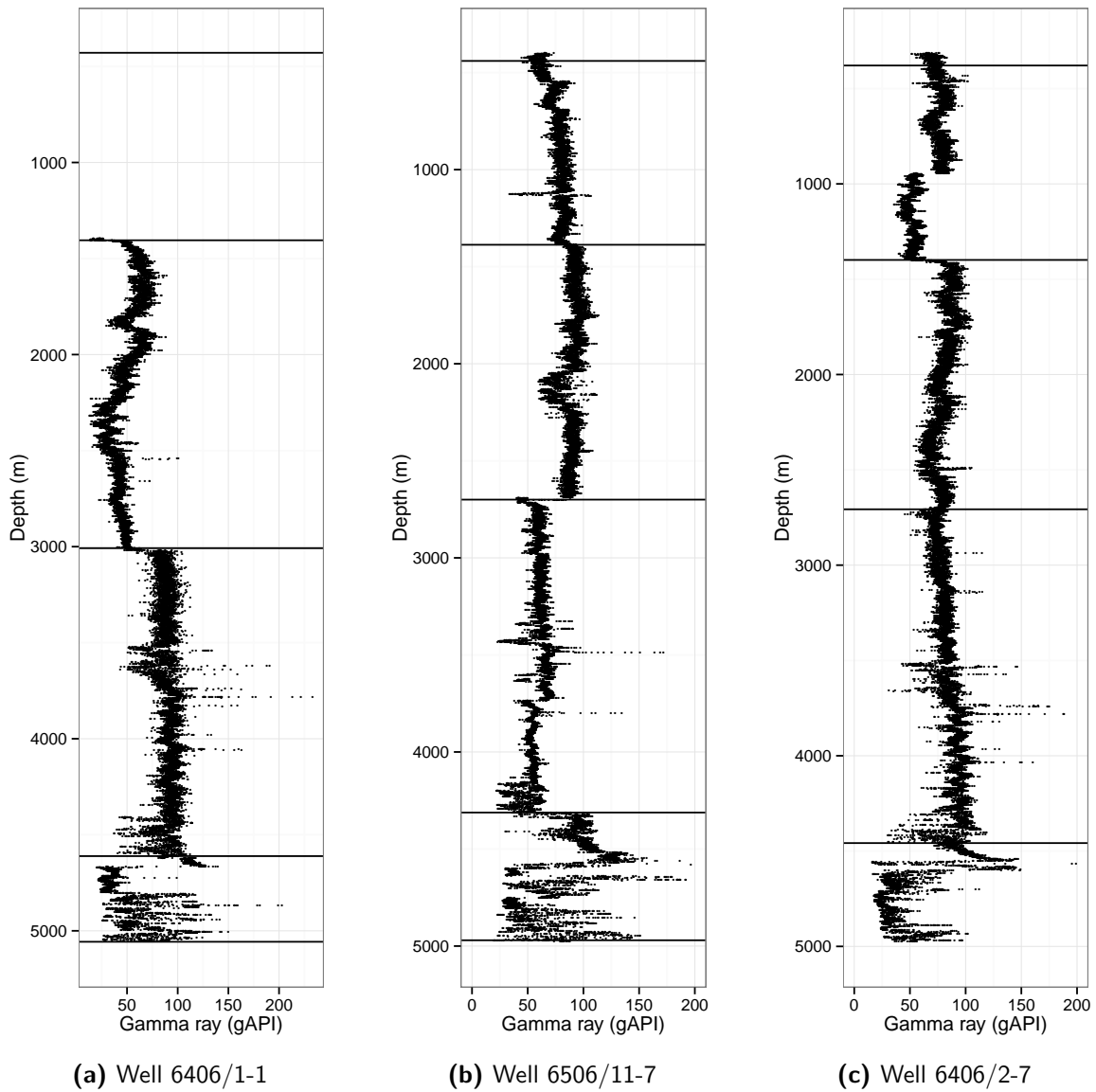
Figure 3: Input GR data and casing points (horizontal lines) for the three mid-Norway wells.

We do not know what environmental corrections, if any, have already been made on these GR logs, and this gives another reason for preferring our data-based approach to a deterministic one. In this section we demonstrate the shifted GR method, and in Section 5.4 we use other available wireline log data to validate the assumption that the casing change is in a consistent shale, as described in Section 4.

5.1 Well 6406/1-1

For well 6406/1-1 there are two casing points where we have sufficient GR data, and these are at 3008m and 4611m rKB. Figure 4 shows samples from the posterior distribution at these points. The input parameter values are as given in Section 3.1 and three parallel chains were used in the Gibbs sampler.

(a) Casing change at 3008m.

(b) Mean = 33.4, SD = 0.67

(c) Casing change at 4611m

(d) Mean = 26.8, SD = 0.97
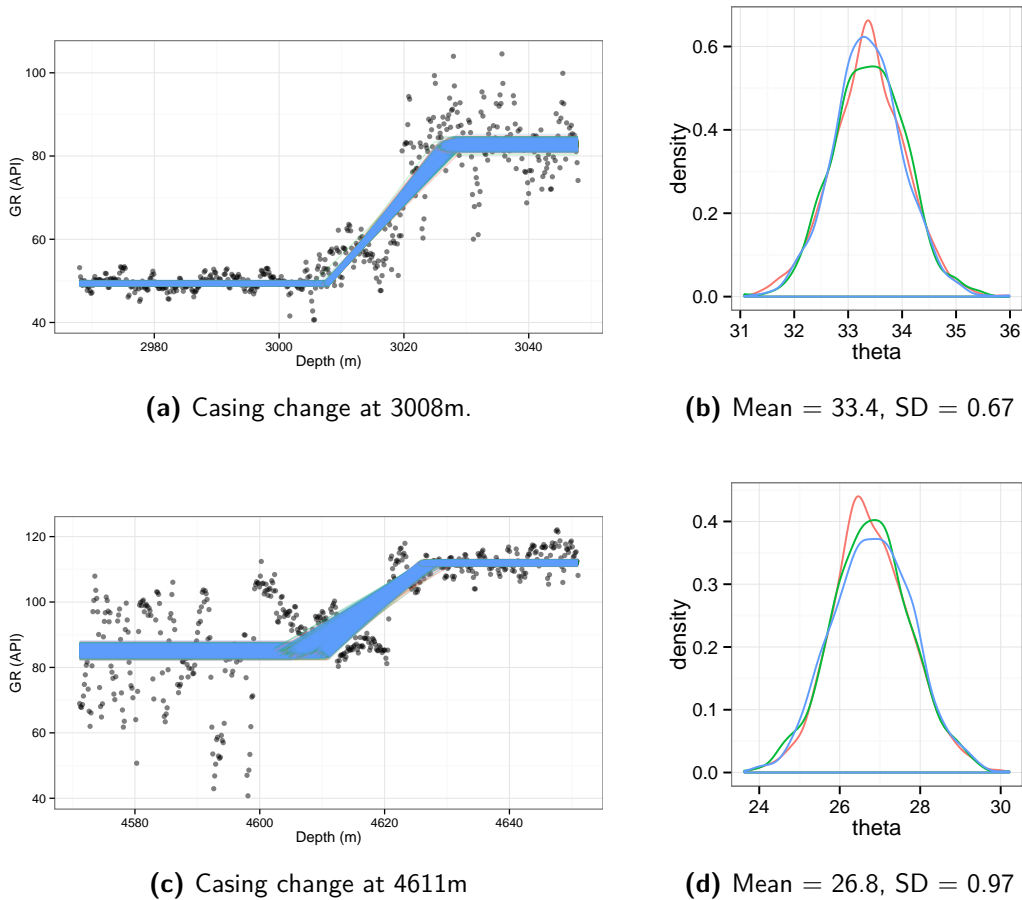
Figure 4: Fitted curves from the Gibbs Sampler (left hand plots) and posterior density samples for the shift parameter θ (right hand plots) for well 6406/1-1. These use the model outlined in Section 3.1.

The left hand plots in each case show the GR data (points), the casing point depth (vertical line) and a random sample of 100 fitted curves from the 3000 samples from the posterior distribution given by

the Gibbs sampler. We ran three parallel chains (see appendix) in each case, giving three independent estimates of all model parameters. The density plots on the right show the posterior densities for the shift parameter θ, with different colours indicating the three independent estimates. Table 1 gives summaries of the posterior distribution of each parameter.

Parameter	Mean	SD	Min	Max	Parameter	Mean	SD	Min	Max
γ_1	49.37	0.22	48.62	50.17	γ_1	85.14	0.89	81.94	88.31
θ	33.41	0.65	31.27	35.79	θ	26.85	0.94	23.65	30.92
z_{dtop}	3007.88	0.16	3006.29	3007.97	z_{dtop}	4609.08	2.24	4602.22	4611.06
z_{dbot}	3027.54	0.79	3024.73	3030.07	z_{dbot}	4626.78	0.83	4625.24	4631.64
τ_v	0.08	0.007	0.059	0.115	τ_v	0.004	0.0004	0.003	0.006
τ_w	0.014	0.002	0.008	0.021	τ_w	0.01	0.002	0.006	0.017
τ_z	0.017	0.002	0.011	0.024	τ_z	0.062	0.007	0.04	0.093

Table 1: Summaries of posterior distributions for well 6406/1-1 at 3008m (left) and 4611m (right).

In all cases the model is clearly working in terms of finding suitable fits to the data. The posterior distributions for each chain, shown by different colours in the density plots, match fairly well, giving us confidence that the Gibbs sampler has converged.
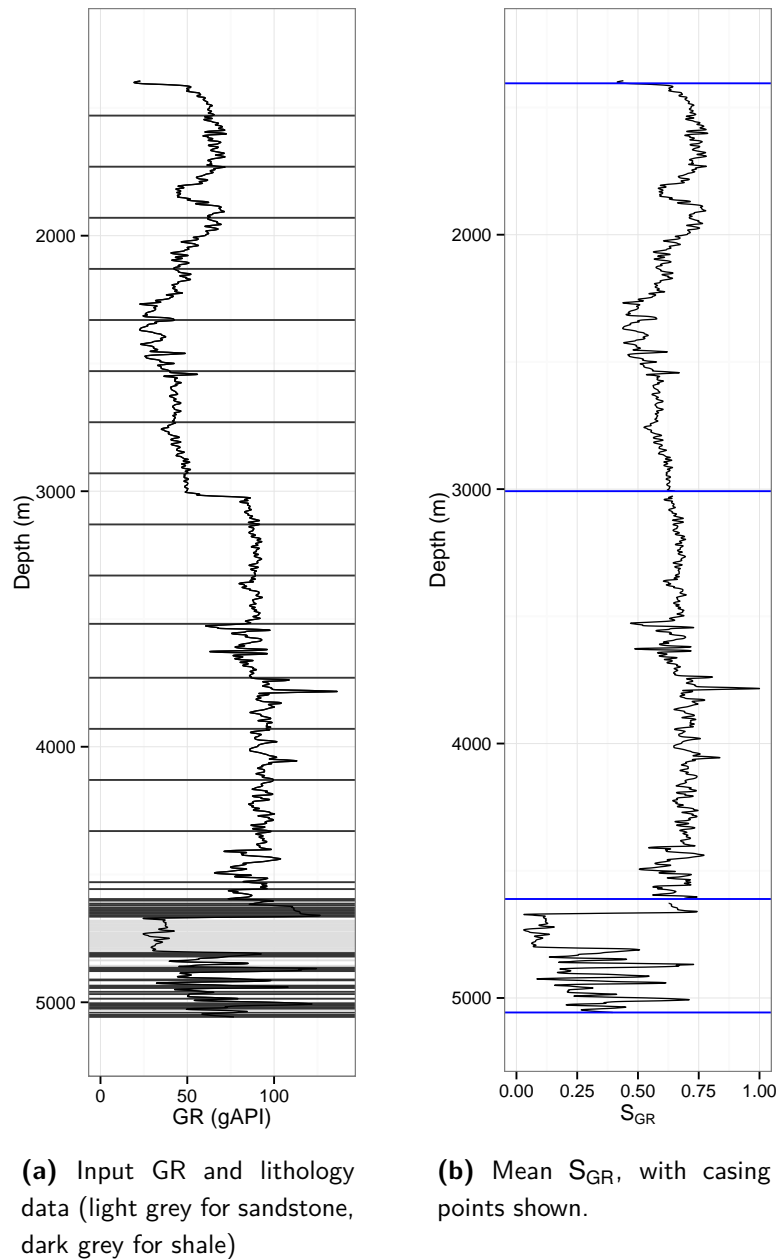
The method can be sensitive to the values for d_{max}, d_{min}, a, b and μ_p. For example, Figure 5 shows the fitted functions for two different values of d_{max}. The light grey lines were found using $d_{max} = 40$, as in Figure 4a. The dark grey lines were found by reducing d to 20. This removes most of the GR log below z_{cas} that is at the stable level, and so the model very easily fits the level using data that should be part of the transition-zone. The end of well report shows that the mud type was changed at 3016m, and this can sometimes cause a jump in the GR log, as it appears to here.
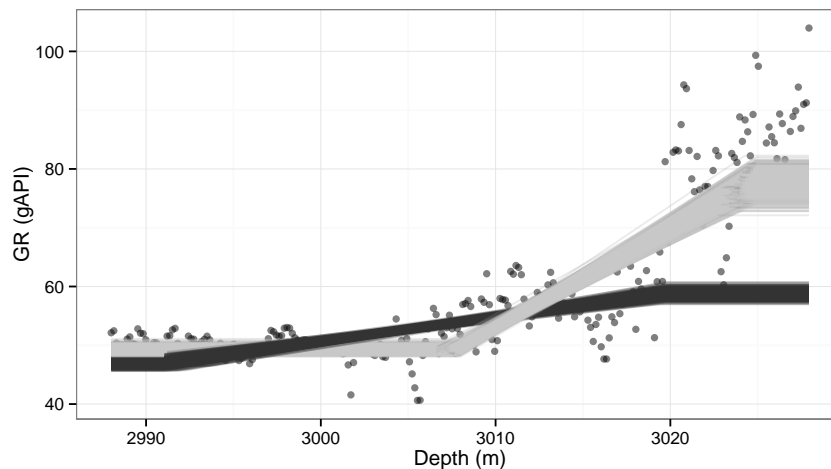
Figure 5: Casing change at 3008m with $d_{max} = 20$ (dark grey lines) and $d_{max} = 40$ (light grey lines).

If the number of iterations were high enough, all three chains would converge to the same distribution, but this early result indicates that this distribution would not be appropriate.

Figure 6 allows us to compare the final result (Fig. 6b) with the input GR (Fig. 6a). Figure 6a also shows the lithology data available, with dark grey horizontal lines denoting shale and light grey denoting sandstone. The lithological markers were obtained mostly from cutting samples, and while there may therefore be some error in their depths, the shales appear consistent. Again we are reassured that the casing points are in shales.

(a) Input GR and lithology data (light grey for sandstone, dark grey for shale)

(b) Mean S_{GR}, with casing points shown.

Figure 6: Smoothed GR log and mean shifted GR index, S_{GR}, for well 6406/1-1.

5.2 Well 6506/11-7

For well 6506/11-7 there are three casing points where we have sufficient GR data, and these are at 1387m, 2700m and 4312m RKB. The GR log behaviour at 2700m is somewhat surprising, as ordinarily one would expect an increase in GR with a smaller borehole diameter. However, the mud log shows that the mud type was changed at 2710m, from a KCI/polymer/glycol mud to a Versapro mineral oil based mud.

Figure 7 shows the posterior samples for the fitted functions (left) and posterior densities for (right) at each of these casing points. Table 2 summarises the posterior distributions for each parameter at each casing point.

Parameter	Mean	SD	Min	Max
γ_1	74.54	0.48	73.06	76.21
θ	16.82	0.63	14.56	19.4
z_{dtop}	1360.17	0.21	1360.07	1361.74
z_{dbot}	1401.79	1.97	1396.79	1413.25
τ_v	0.004	0.001	0.001	0.011
τ_w	0.066	0.006	0.049	0.088
τ_z	0.055	0.008	0.029	0.088

Parameter	Mean	SD	Min	Max
γ_1	84.33	0.73	81.41	86.84
θ	-33.92	0.84	-36.99	-30.98
z_{dtop}	2689.73	0.39	2686.4	2690.06
z_{dbot}	2703.63	0.15	2703.32	2704.69
τ_v	0.016	0.002	0.01	0.025
τ_w	0.002	0.0003	0.001	0.003
τ_z	0.032	0.003	0.021	0.047

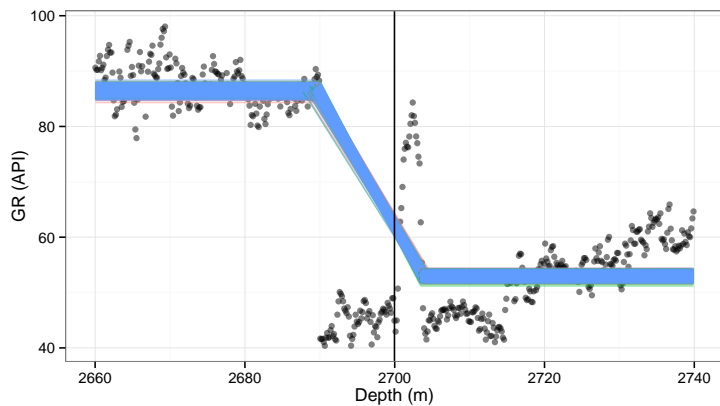| Parameter	Mean	SD	Min	Max
γ_1	47.03	0.67	44.8	49.38
θ	38.84	1.88	32.69	44.77
z_{dtop}	4311.81	0.28	4310.23	4312.05
z_{dbot}	4322.52	2.57	4316.63	4327.45
τ_v	0.012	0.001	0.008	0.017
τ_w	0.004	0.002	0.002	0.012
τ_z	0.004	0.001	0.002	0.006

Table 2: Summaries of posterior distributions for casing points in well 6506/11-7 at 1387m (top left), 2700m (top right) and 4312m (bottom).
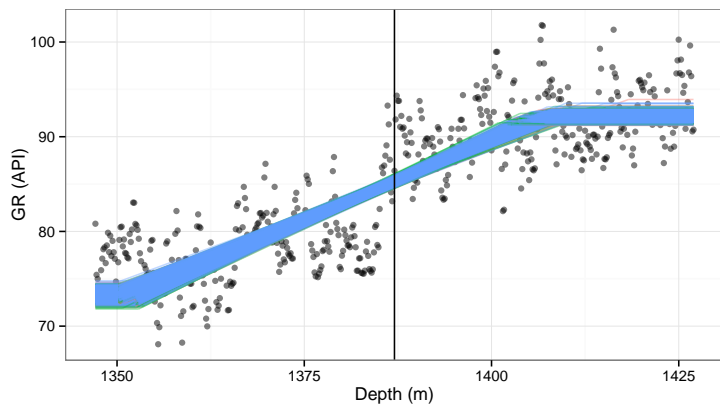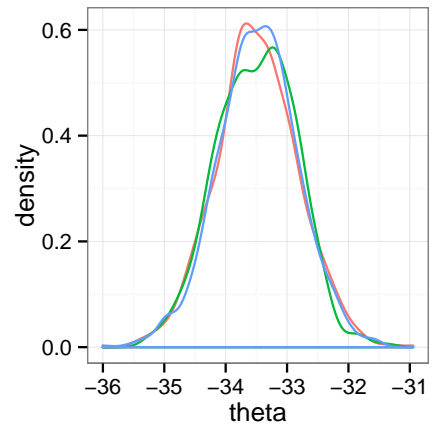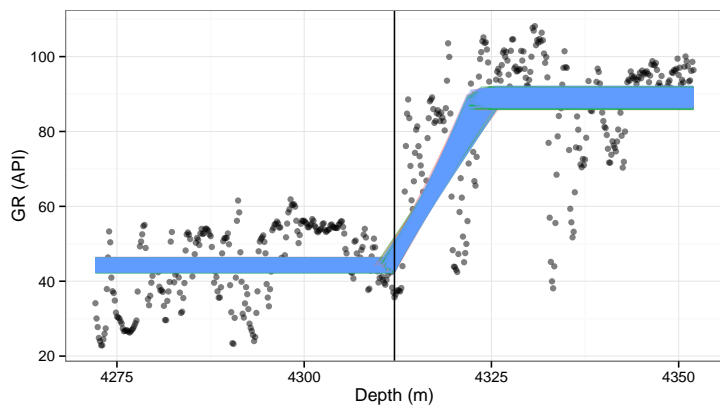
(a) Casing change at 1387m
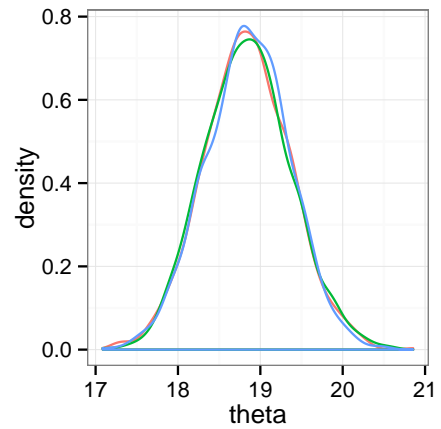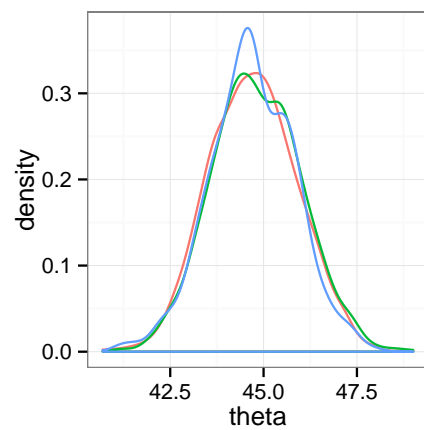
(b) Mean = 18.8, SD = 0.54

(c) Casing change at 2700m

**(d)** Mean = -33.5, SD = 0.67

(e) Casing change at 4312m

(f) Mean = 44.8, SD = 1.12

Figure 7: Fitted curves from Gibbs Sampler (left hand plots) and posterior density samples for the shift parameter θ (right hand plots) for well 6506/11-7. These use the model outlined in Section 3.1.

Again, the Gibbs sampler's chains appear to have converged, and the fitted curves appear to fit the GR data well.

Figure 8 demonstrates another feature of this shifted GR method, which is that it will not necessarily produce distributions that focus in on one curve. Here, the posterior distribution appears to favour two different values of z_{dbot} more or less equally. For this reason the posterior mean for z_{dbot} in Table 2 lies between the two values, and the SD and range are large.
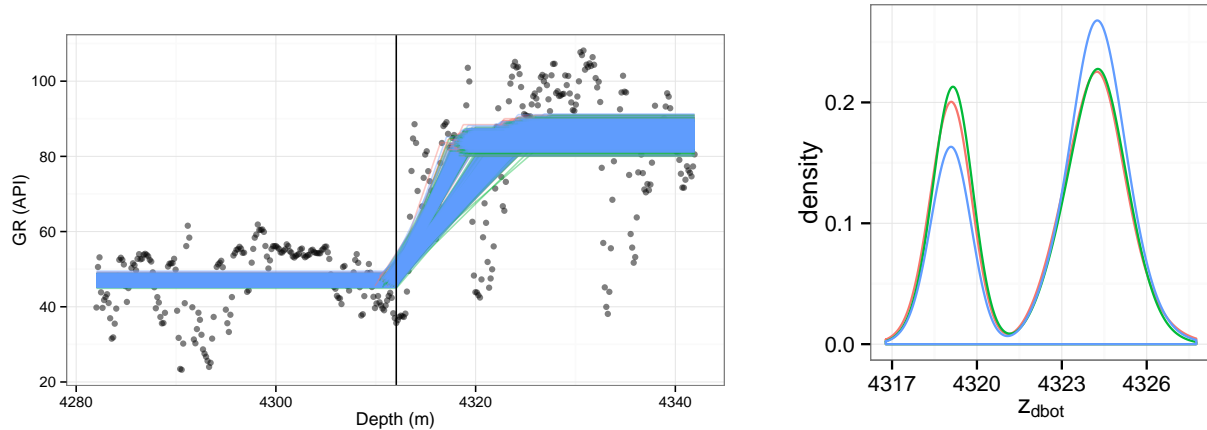

Figure 8: The casing change at 4312m in well 6506/11-7, with posterior function fits (left), and the posterior samples from z_{dbot} (right).

This is not necessarily a problem, particularly since here it results only in a slight difference in the width of the transition-zone (the posterior values for γ_1 and θ are still very similar). If the difference was more serious, for example in the value of θ, then it may be wise to look further into the other wireline logs and the well report to try to understand whether one solution is more realistic.

Figure 9 compares the input GR (left, with lithology data also shown) with the mean S_{GR} found using our method.
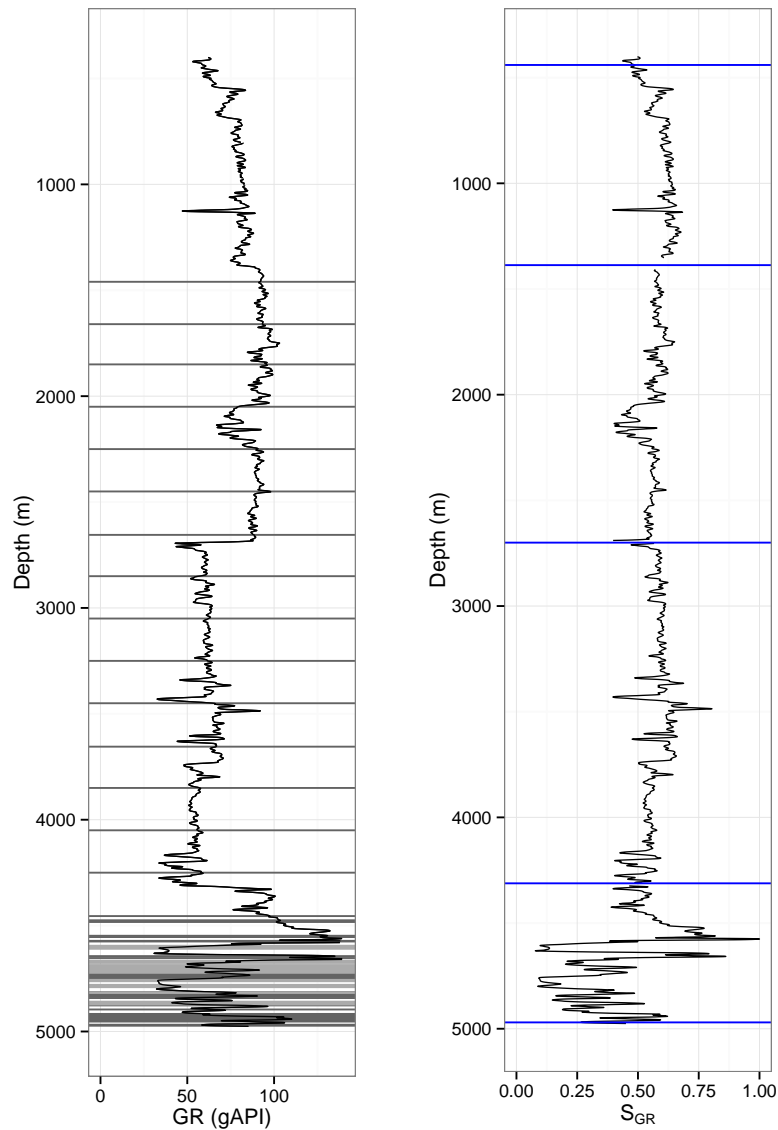
(a) Input GR and lithology data (light grey for sandstone, dark grey for shale)

(b) Mean S$_{GR}$

Figure 9: Input GR log and mean shifted GR index, S$_{GR}$, for well 6506/11-7.

5.3 Well 6406/2-7

For well 6406/2-7 there are four casing changes with GR data, at 379m, 1399m, 2707m and 4458m. The posterior function fits are shown in Figure 10, along with posterior densities for θ. Table 3 summarises the posterior densities for each parameter at each casing point.

Some of the shifts in GR are much more gradual in this well, particularly that at 379m.

Parameter	Mean	SD	Min	Max
γ_1	69.55	0.35	68.31	70.79
θ	3.73	0.5	2.25	5.32
z_{dtop}	342.5	0.19	342.2	343.7
z_{dbot}	395.2	2.63	379.4	398.6
τ_v	0.005	0.001	0.002	0.013
τ_w	0.085	0.007	0.059	0.115
τ_z	0.05	0.007	0.032	0.078

Parameter	Mean	SD	Min	Max
γ_1	52.09	0.33	50.86	53.26
θ	34.64	0.51	32.96	36.46
z_{dtop}	1397.6	0.72	1395.1	1398.9
z_{dbot}	1416.2	0.49	1413.7	1418.1
τ_v	0.037	0.003	0.025	0.05
τ_w	0.045	0.006	0.03	0.074
τ_z	0.042	0.005	0.027	0.062

Parameter	Mean	SD	Min	Max
γ_1	84.11	0.36	82.84	85.43
θ	-10.86	0.66	-14.01	-8.69
z_{dtop}	2670.1	0.09	2670.1	2670.9
z_{dbot}	2709.1	0.47	2707.3	2713.2
τ_v	0.003	0.001	0.001	0.008
τ_w	0.116	0.012	0.067	0.164
τ_z	0.016	0.002	0.01	0.023

| Parameter	Mean	SD	Min	Max
γ_1	80.45	0.68	77.79	82.8
θ	14.25	1.01	10.47	17.98
z_{dtop}	4454.9	0.25	4453.8	4457.8
z_{dbot}	4491.7	1.72	4486.4	4494.9
τ_v	0.004	0.0004	0.003	0.005
τ_w	0.026	0.003	0.017	0.036
τ_z	0.049	0.012	0.016	0.114

Table 3: Summaries of posterior distributions for casing points in well 6406/2-7 at 379m (top left), 1399m (top right), 2707m (bottom left) and 4458m (bottom right).
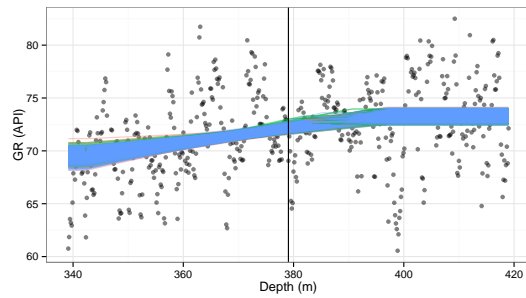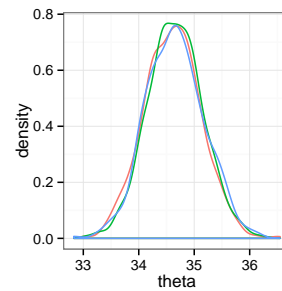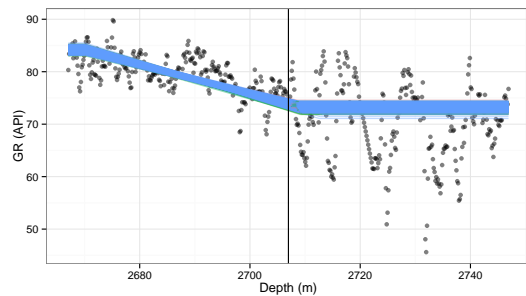
(a) Casing change at 379m
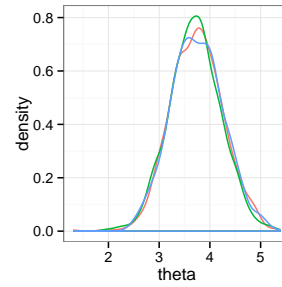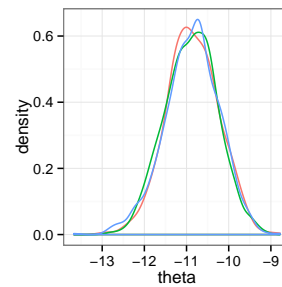
(b) Mean = 3.73, SD = 0.50
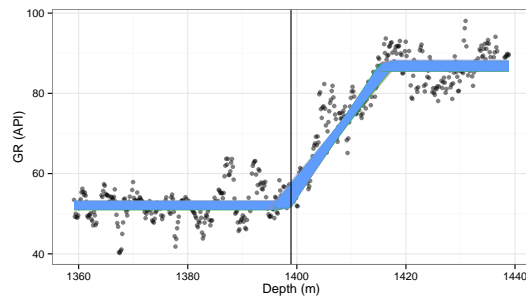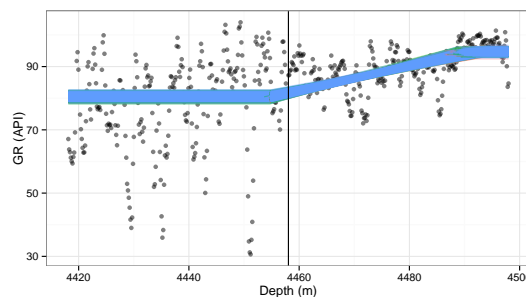
(c) Casing change at 1399m
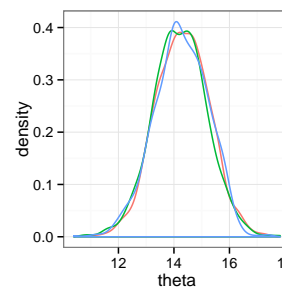
(d) Mean = 34.6, SD = 0.51

**(e)** Casing change at 2707m

(f) Mean = -10.9, SD = 0.66

(g) Casing change at 4458m

(h) Mean = 14.3, SD = 1.0

Figure 10: Fitted curves from Gibbs Sampler (left hand plots) and posterior density samples for the shift parameter θ (right hand plots) for well 6406/2-7. These use the model outlined in Section 3.1.

19

Figure 11 compares the smoothed GR data with the mean S_{GR}, this time without lithology data.


(a) Input GR data   **(b)** Mean S_{GR}
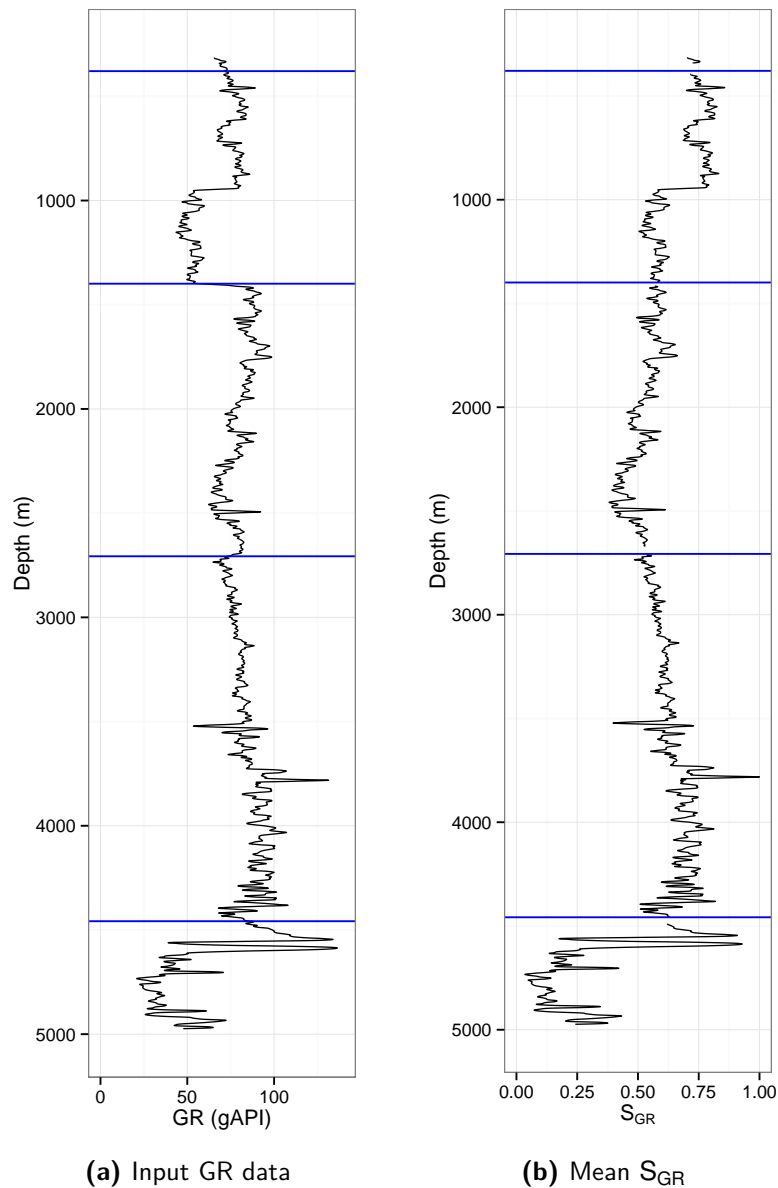
Figure 11: Input GR log and mean shifted GR index, S_{GR}, for well 6406/2-7.

5.4 Example: validating our assumptions

To verify that the shifted GR model is appropriate, we use some of the approaches mentioned in Section 4 on the data from the three mid-Norway offshore wells to see whether the lithology around each casing change is consistent. There is often little choice of wireline log in the shallower sections of the well, and so the choice of logs depends on which logs are available.
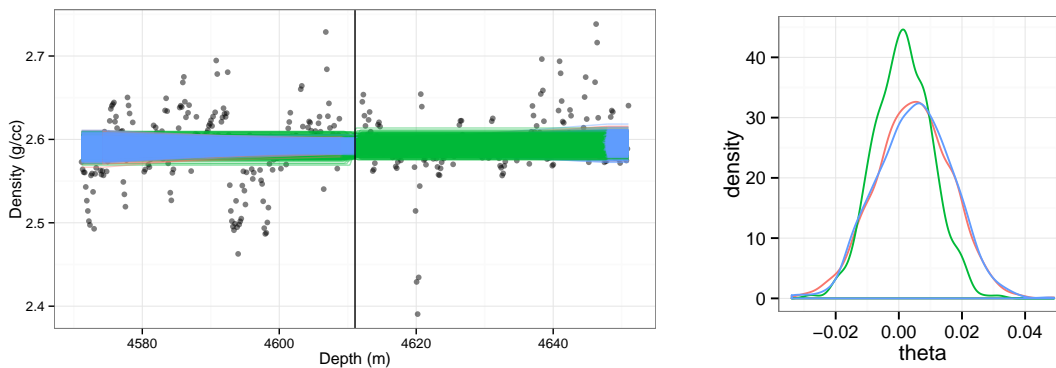
5.4.1 Well 6406/1-1

The only other wireline log available around 3008m is resistivity. Hearst et al. (2000) states that resistivity does change with lithology, even though this change is complicated by other factors, such as fluid content. Figure 12 shows the resistivity around 3008m, with a fitted linear model of resistivity against depth shown in blue. The gradient coefficient in the linear regression of resistivity against depth is estimated to be -2.8×10^{-4}Ohm.m/m which is not significant under the linear regression model (the t statistic is -1.7, which has a p-value of 0.09). This supports the notion that the lithology is consistent, and the resistivity values themselves are consistent with shale.
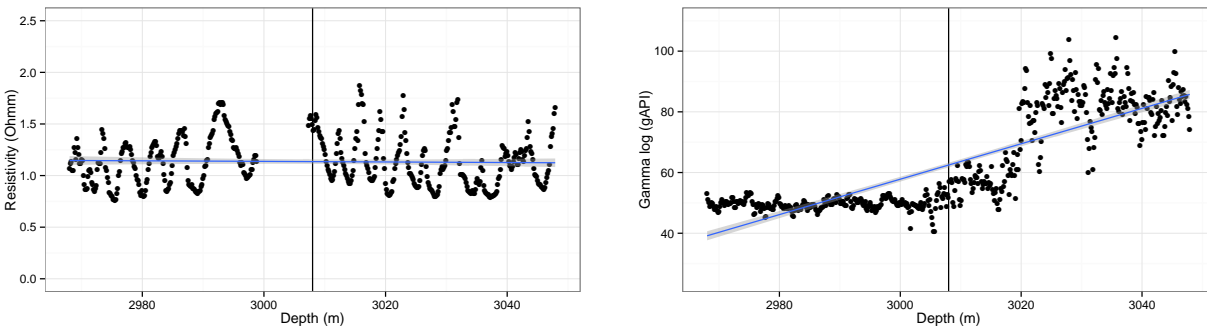
Figure 12: Deep resistivity (left) and GR (right) around 3008m, with linear regression fits shown.

Figure 13 shows the density log around the casing change at 4611m in well 6406/1-1, with the posterior samples of the fitted model function, and the posterior samples of θ.

Figure 13: Density log for well 6406/1-1 around the casing point at 4611m, with the posterior function fits (left), and posterior samples for the shift parameter θ. The different coloured lines represent different chains from the Gibbs sampler.

The density does not show any sign of change over this region, and again this supports a consistent lithology.

5.4.2 Well 6506/11-7

Most of the wireline logs were recorded only below the casing point at 1387m, so again we have only resistivity for the shallowest casing point. Figure 14 shows the resistivity around the casing point, with a linear regression fit in blue. Again, the coefficient of depth in a linear regression of resistivity against depth is non-significant (the t statistic is -1.6 which has a p-value of 0.11).
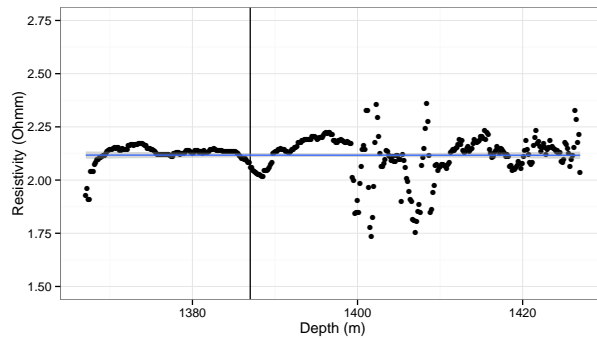
Figure 14: Deep resistivity around 1387m, with a linear regression fit shown.

Figure 15 shows the neutron porosity (in limestone units) and density logs around the casing point at 4312m separately, and both show slight trends with depth.
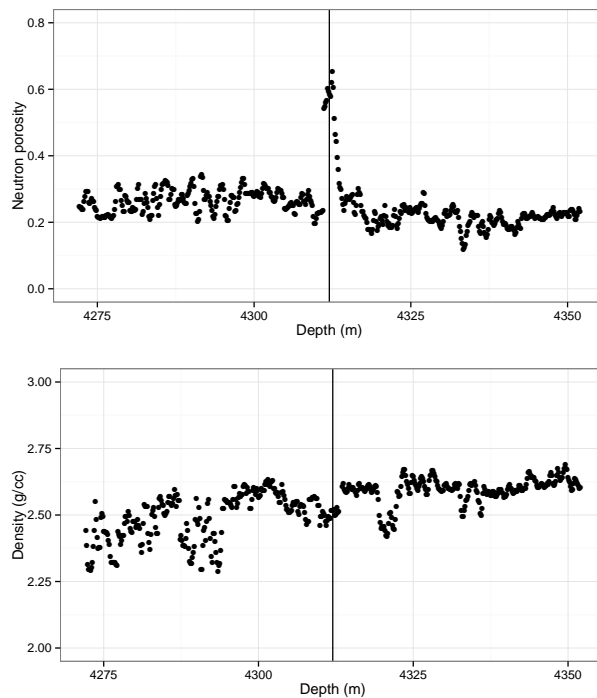
Figure 15: Neutron porosity (top) and density (bottom) around the casing point at 4312m (shown by vertical line). There is a clear spike in porosity at the casing point, and a slight trend in both logs.

Figure 16 shows the neutron-density combination plot around the casing change at 4312m in well 6506/11-7, as in Rider (1996). The alignment of the scales results in both curves overlapping in water-filled limestone porosity. Below 4292m the data appear to be shale as indicated by the characteristic separation between the curves, with NPHI reading a considerably higher porosity than RHOB.
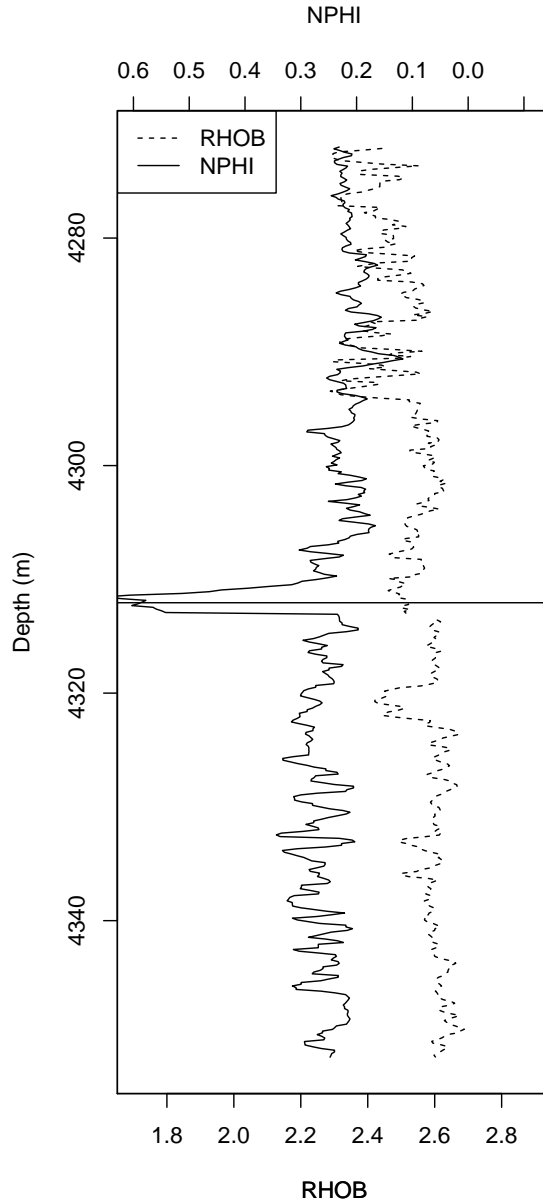


Figure 16: Neutron porosity (solid) and density (dashed) around the casing point at 4312m (shown by black line).There is a clear spike in porosity at the casing point, and a slight trend in both logs, consistent with a gradual reduction in porosity with increasing depth.

5.4.3 Well 6406/2-7

Again, for the casing changes at 379m and 1399m there are few wireline logs, but below this depth both neutron and density are available. Figure 17 shows the neutron and density plotted against depth around the casing points at 2707m and 4458m. Although the data are not in the same regions of the plots, the separations between the logs are consistent with shale and show similar lithology above and below the casing point.
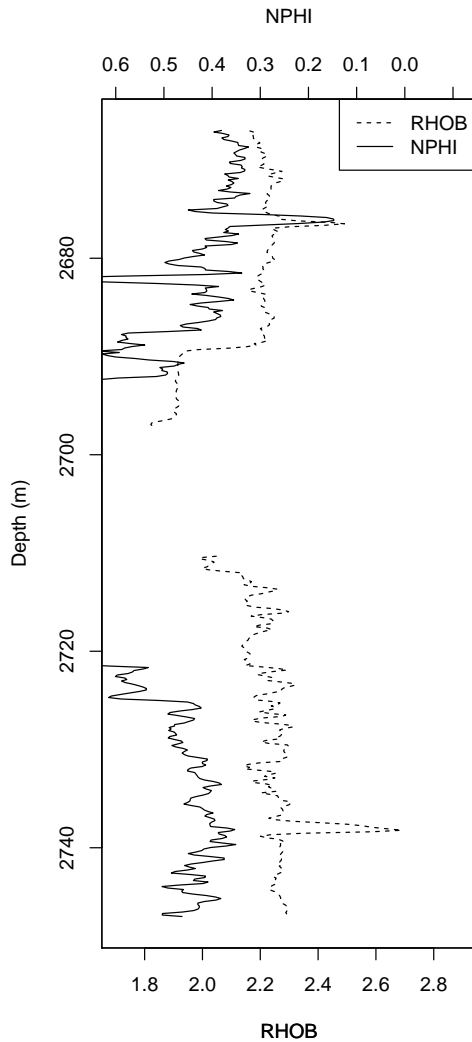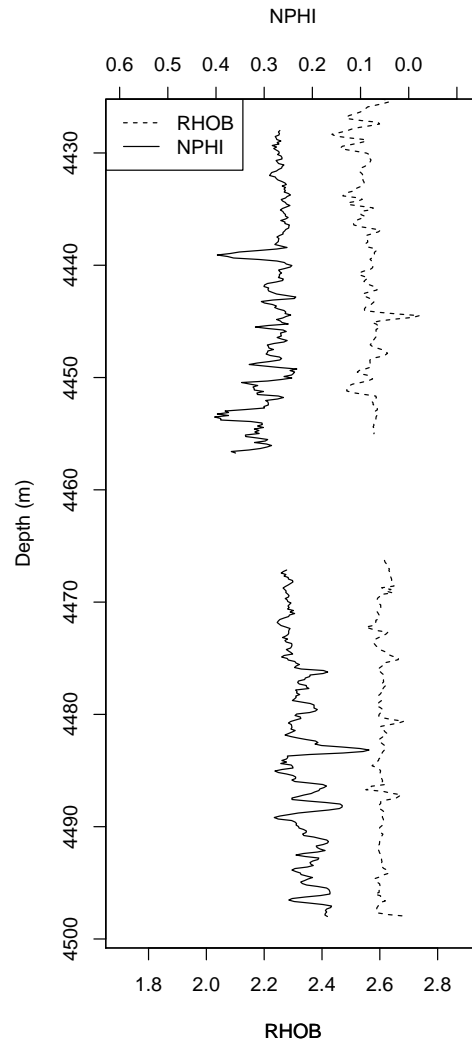
(a) Well 6406/2-7, 2707m   **(b)** Well 6406/2-7, 4458m

Figure 17: Neutron-density plots for two casing changes from well 6406/2-7, at 2707m (left) and 4458m (right). Both are consistent with shale, though the data around 2707m are more variable, possibly due to hole wash-out around the casing point.

6 Discussion

The problem we have addressed is that of detecting a shift in mean response at a specified casing point. In the statistical literature, this is a changepoint problem (Krishnaiah and Miao, 1988), with the added complication that in all the examples we have seen the change in shift is not instant but takes place over an interval or transition-zone. These zones vary in length from example to example. Moreover, the observations within the transition zone tend to transit to the new level unpredictably and with higher variability than preceding and succeeding observations. The typical industry approach to this problem is to make a "by eye" adjustment for shift, and to ignore the transition zone. The method described here is a statistical formalisation of that process.

We adopt a Bayesian approach as the most appropriate, extending from the changepoint problem discussed by Carlin et al. (1992), who also give a brief introduction to the Gibbs sampler. One advantage of the Bayesian approach is that it can incorporate expert judgements as to the process - for example, in the depth of the transition-zone. Another advantage is that it can handle uncertainties for the different kinds of quantities involved: depth of transition-zone, variation in mean shift, and so forth. The results produced are posterior probability distributions for these quantities.

The Bayesian approach requires parameters to control the estimation process. These can be chosen subjectively according to the problem at hand, but we also suggest defaults which we have found to work well in practice. Typically, the defaults are based on non-informative prior distributions, where we would expect data to dominate the prior formulation very quickly.

The use of a Markov Chain Monte Carlo mechanism such as the Gibbs sampler, as described in the Appendix, is standard in such settings. The algorithm we present is implemented in the statistical language R (R Development Core Team, 2011), making use of R packages rjags (Plummer, 2014) and R2Jags (Su and Yajima, 2014). All our examples run automatically with default parameters and take a few minutes each on a desktop PC. In addition to providing a formal statistical basis for the alignment of GR segments between casing points, this method should provide results which are faster, more reliable, more automatic, and less biased than those produced by manual manipulations of the GR log. Further, the procedure is transparent and with assumptions which may be challenged and pursued via diagnostics at a finer level of detail, if so desired. We would expect such a tool to be used with expert oversight rather than to provide unchecked fully automated realignments.

Except diagnostically, we do not presently make use of uncertainties attached to the mean shift or to segments joining the casing points. However, elsewhere we are constructing stochastic dynamic Bayesian networks which model pore pressure layer by layer as we descend through the earth. The shifted GR index is an important ingredient to this modelling process. The availability of uncertainties attached to features in the shifted GR index is essential in that context.

7 Summary

We have presented a Bayesian, data-based approach for accounting for uncertainty in the open-hole GR log around casing changes. This method relies on the assumption that the lithology around the casing point is consistent, and we have shown some methods for validating this using other wireline logs. The shifted GR method does not rely on any parameters relating to borehole conditions, mud type and so on, but does require careful consideration from the user. Using the posterior distributions obtained through the probability model, we are able to asses our uncertainty about the fit (given the model). Although the mathematics is unavoidably complex, they can be implemented in software, and an R package is in development for release to the community.

References

Asquith, G. & Krygowski D. 2004. *Basic Well Log Analysis* (2 ed.). AAPG.

Bhuyan, K. & Passey Q. 1994. Clay estimation from GR and neutron-density porosity logs. In *SPWLA 35th Annual Logging Symposium*.

Bristow, C. & Williamson B. 1998. Spectral gamma ray logs: core to log calibration, facies analysis and correlation problems in the southern north sea. *Geological Society, London, Special Publications* **136**, 1–7.

Carlin, B. P., Gelfand A. E., & Smith A. F. 1992. Hierarchical bayesian analysis of changepoint problems. *Applied Statistics* **41**, 389–405.

Carlin, B. P. & Louis T. 2009. *Bayesian methods for data analysis*. Boca Raton: Chapman & Hall.

Casella, G. & George E. I. 1992. Explaining the gibbs sampler. *Journal of the American Statistical Association* **46**, 167–174.

Chen, W.-F. 1998. Gamma-log trend facies in the choshui fan-delta, taiwan. *Terr. Atmos. Oceanic Sci* **9**, 633–642.

Clouzea, F., Hansen R., & Prouvost L. 1998. Planning and drilling wells into the next millennium.

Devereux, S. 1998. *Practical Well Planning and Drilling Manual*. PennWell.

Eaton, B. A. 1975. The equation for geopressure prediction from well logs. In *Fall Meeting of the Society of Petroleum Engineers of AIME*. Society of Petroleum Engineers.

Gelfand, A. E., Smith A. F., & Lee T.-M. 1992. Bayesian analysis of constrained parameter and truncated data problems using gibbs sampling. *Journal of the American Statistical Association* **87**, 523–532.

Hearst, J. R., Nelson P. H., & Paillett F. L. 2000. *Well logging for physical properties*. Wiley.

Krishnaiah, P. & Miao B. 1988. Review about estimation of change points. In P. Krishnaiah and C. Rao (Eds.), *Handbook of Statistics*, Volume 7, pp. 375–402. Amsterdam: North-Holland: Elsevier.

Lehmann, K. 2010. Environmental corrections to gamma-ray log data: Strategies for geophysical logging with geological and technical drilling. *Journal of Applied Geophysics* **70**, 17–26.

Littleton, R., Cody R., & Landreth J. 2002. Pre-drill seismic predictions platform (pore pressure, fracture gradient, lithology, and pore fluids) effectively used as a well planning tool by a multi-discipline deepwater operations team.

Maučec, M., Hendriks P., Limburg J., & de Meijer R. 2009. Determination of correction factors for borehole natural gamma-ray measurements by monte carlo simulations. *Nuclear Instruments and Methods in Physics Research A* **609**, 194–204.

Mendoza, A., Ellis D., & Rasmus J. 2006. Why the LWD and Wireline Gamma Ray Measurements May Read Different Values in the Same well. *Society of Petroleum Engineers* **SPE 101718**.

Mouchet, J. & Mitchell A. 1989. *Abnormal Pressures While Drilling*. Manuels Techniques Elf Aquitaine.

Plummer, M. 2014. *rjags: Bayesian graphical models using MCMC*. R package version 3-13.

R Development Core Team 2011. *R: A Language and Environment for Statistical Computing*. Vienna, Austria: R Foundation for Statistical Computing. ISBN 3-900051-07-0.

Rider, M. 1990. Gamma-ray log shape used as a facies indicator: critical analysis of an oversimplified methodology. *Geological Society, London, Special Publications* **48**, 27–37.

Rider, M. 1996. *The Geological Interpretation of Well Logs* (second ed.). Whittles.

Serra, O. & Serra B. 2004. *Well Logging: data acquisition and application*. Serralog.

Stromswold, D. C. & Wilson R. D. 1981. Calibration and data correction techniques for spectral gamma-ray logging. *SPWLA twenty-second annual logging symposium*.

Su, Y.-S. & Yajima M. 2014. *R2jags: A Package for Running jags from R*. R package version 0.04-01.

Swarbrick, R. E. 2002. Challenges of porosity-based pore pressure prediction. *CSEG Recorder* **75**.

Thibal, J., Etchecopar A., Pozzi J., Barthès V., & Pocachard J. 1999. Comparison of magnetic and gamma ray logging for correlations in chronology and lithology: example from the Aquitanian Basin (France). *Geophysical Journal International* **137**, 839–846.

Weatherford 2009. *Wireline Services Log Interpretation Chart Book*.

Zhang, J. 2011. Pore pressure prediction from well logs: Methods, modifications, and new approaches. *Earth-Science Reviews* **108**, 50–63.

A The Gibbs sampler

When trying to solve a problem in the Bayesian framework, the desired end result is usually a marginal posterior distribution. For instance, in the GR shift problem described in this report, we would like to know the marginal posterior distribution for θ, the probability of θ conditional on the data. Finding this distribution analytically would involve some prohibitively complicated integration. The Gibbs sampler provides a way to obtain random samples from posterior marginal distributions without ever having to solve these integrals, by sampling from the conditional distributions.

The Gibbs Sampler has been popular since the 1980s, and has been used in a wide array of problems (Gelfand et al., 1992). It is an iterative sampling scheme and proceeds in the following way. We write $\Theta = \{\theta_1, \ldots, \theta_k\}$ to denote the collection of all the model's parameters, and D for the data. We start with an arbitrary set of values $\Theta^{(0)} = \left(\theta_1^{(0)}, \ldots, \theta_k^{(0)}\right)$. We then draw $\theta_1^{(1)}$ from the distribution

$$\theta_1 \mid \theta_2^{(0)}, \ldots, \theta_k^{(0)}, D.$$

and then $\theta_2^{(1)}$ from

$$\theta_2 \mid \theta_1^{(1)}, \theta_3^{(0)}, \ldots, \theta_k^{(0)}, D,$$

and so on, until we have drawn $\theta_k^{(1)}$ from

$$\theta_k \mid \theta_1^{(1)}, \ldots, \theta_{k-1}^{(1)}, D.$$

This gives us a new set of values $\Theta^{(1)}$. We repeat this process, in general sampling $\theta_i^{(j)}$ from

$$\theta_i \mid \theta_1^{(j)}, \ldots, \theta_{i-1}^{(j)}, \theta_{i+1}^{(j-1)}, \ldots, \theta_k^{(j-1)}, D$$

until we have several thousand or more such $\Theta^{(j)}$. Under fairly general conditions, the distribution of these samples tends towards the true posterior distribution. Although eventual convergence can be proved, it is not possible to calculate how many iterations there should be before it is reached. Therefore several precautions are often taken (Carlin and Louis, 2009).

- **Burn-in**: the first m sets $\Theta^{(i)}$ are discarded, to remove dependence on the initial value $\Theta^{(0)}$.

- **Parallel chains**: several independent sequences are generated, rather than just one. In practice, this means re-running the full estimation procedure several times. If the results have very similar properties, this suggests the samples can be trusted.

- **Thinning**: this deals with the problem of the chain getting stuck in particular areas, and not exploring the full probability space properly, which is particularly a problem where there are local maxima separated by regions of very low probability. The sequence of values $\Theta^{(j)}$ is 'thinned' by keeping only every n^{th} set.

Once the final collection of samples has been found, samples of the marginal posteriors are given by the values of each parameters. Population properties can be estimated using the samples; for example, the mean of θ_1 can be approximated by the mean of the sample values of θ_1, and so on. More detail about the mathematics behind the Gibbs Sampler is given in Casella and George (1992), and Gelfand et al. (1992) give an example. The problem we describe is very similar to the changepoint problem discussed by Carlin et al. (1992), who also give a brief introduction to the Gibbs sampler.